



## Original article

**Advanced imaging for quantification of abnormalities in the salivary glands of patients with primary Sjögren's syndrome**

Pilar Jimenez-Royo<sup>1</sup>, Michele Bombardieri<sup>2</sup>, Coziana Ciurtin <sup>3</sup>, Michalis Kostapanos<sup>4,5</sup>, Anwar R. Tappuni<sup>6</sup>, Natasha Jordan<sup>7</sup>, Azeem Saleem<sup>8,9,\*</sup>, Teresa Fuller<sup>1</sup>, Kathleen Port<sup>1</sup>, Elena Pontarini<sup>2</sup>, Davide Lucchesi<sup>2</sup>, Robert Janiczek<sup>1</sup>, Paul Galette<sup>1</sup>, Graham Searle<sup>8,\*</sup>, Neel Patel<sup>1</sup>, Lucy Kershaw<sup>10,11</sup>, Calum Gray<sup>11</sup>, Nirav Ratia<sup>1</sup>, André van Maurik<sup>1</sup>, Marius de Groot<sup>1,4</sup>, Nicolas Wisniacki<sup>1</sup>, Mats Bergstrom<sup>1</sup> and Ruth Tarzi <sup>1</sup>

**Abstract**

**Objectives.** To assess non-invasive imaging for detection and quantification of gland structure, inflammation and function in patients with primary Sjögren's syndrome (pSS) using PET-CT with <sup>11</sup>C-Methionine (<sup>11</sup>C-MET; radiolabelled amino acid), and <sup>18</sup>F-fluorodeoxyglucose (<sup>18</sup>F-FDG; glucose uptake marker), to assess protein synthesis and inflammation, respectively; multiparametric MRI evaluated salivary gland structural and physiological changes.

**Methods.** In this imaging/clinical/histology comparative study (GSK study 203818; NCT02899377) patients with pSS and age- and sex-matched healthy volunteers underwent MRI of the salivary glands and <sup>11</sup>C-MET PET-CT. Patients also underwent <sup>18</sup>F-FDG PET-CT and labial salivary gland biopsies. Clinical and biomarker assessments were performed. Primary endpoints were semi-quantitative parameters of <sup>11</sup>C-MET and <sup>18</sup>F-FDG uptake in submandibular and parotid salivary glands and quantitative MRI measures of structure and inflammation. Clinical and minor salivary gland histological parameter correlations were explored.

**Results.** Twelve patients with pSS and 13 healthy volunteers were included. Lower <sup>11</sup>C-MET uptake in parotid, submandibular and lacrimal glands, lower submandibular gland volume, higher MRI fat fraction, and lower pure diffusion in parotid and submandibular glands were observed in patients vs healthy volunteer, consistent with reduced synthetic function. Disease duration correlated positively with fat fraction and negatively with <sup>11</sup>C-MET and <sup>18</sup>F-FDG uptake, consistent with impaired function, inflammation and fatty replacement over time. Lacrimal gland <sup>11</sup>C-MET uptake positively correlated with tear flow in patients, and parotid gland <sup>18</sup>F-FDG uptake positively correlated with salivary gland CD20+ B-cell infiltration.

**Conclusion.** Molecular imaging and MRI may be useful tools to non-invasively assess loss of glandular function, increased glandular inflammation and fat accumulation in pSS.

**Key words:** SS, MRI, CT scanning, radionuclide imaging, diagnostic imaging, outcome measures and histopathology

<sup>1</sup>Research and Development, GlaxoSmithKline, Stevenage, <sup>2</sup>Experimental Medicine and Rheumatology, Queen Mary University of London, London, <sup>3</sup>Centre for Adolescent Rheumatology, University College London, London, <sup>4</sup>GlaxoSmithKline Clinical Unit Cambridge, Cambridge, <sup>5</sup>Department of Medicine, Addenbrooke's Hospital, Cambridge University Hospitals NHS Foundation Trust, Cambridge, <sup>6</sup>Institute of Dentistry, Queen Mary University of London, London, <sup>7</sup>Rheumatology Department, Addenbrooke's Hospital, Cambridge University Hospitals NHS Foundation Trust, Cambridge, <sup>8</sup>Invicor, Centre for Imaging Sciences, A Konica Minolta Company, London, <sup>9</sup>Faculty of Health Sciences, University of Hull, Hull, <sup>10</sup>Centre for Inflammation Research, University of Edinburgh and <sup>11</sup>Edinburgh Imaging, University of Edinburgh, Edinburgh  
Submitted 22 April 2020; accepted 21 August 2020

Correspondence to: Ruth Tarzi, Clinical Development, GSK, Stevenage, Hertfordshire SG1 2NY, UK. E-mail: ruth.m.tarzi@gsk.com

**Introduction**

Primary SS (pSS) is a systemic auto-inflammatory rheumatic disease with unknown etiopathogenesis in which the autoimmune reaction targets the salivary and lacrimal glands. Dry mouth (xerostomia) and dry eyes (keratoconjunctivitis sicca) are two of the main symptoms of pSS [1, 2], although multiple organs and mucosal surfaces may be affected [3, 4]. There is currently no disease-modifying drug for pSS, and the disease has a significant detrimental impact on quality of life [5].

### Rheumatology key messages

- We examined  $^{11}\text{C}$ -Methionine,  $^{18}\text{F}$ -FDG PET-CT and multi-parametric MRI for quantitative pSS salivary gland imaging.
- Patients with pSS had structural/functional differences in salivary and lacrimal glands versus healthy volunteers.
- Molecular imaging parameters correlated with disease characteristics, providing initial validation for quantitative assessment of pSS.

Early pSS diagnosis and assessment of disease activity are hampered by non-specific clinical manifestations, subjective symptoms and a lack of specific or quantitative biomarkers. Moreover, standard diagnostic and disease monitoring techniques [6, 7] have drawbacks, including sampling errors from biopsies, and variability in salivary and tear flow assays. Although salivary gland ultrasound has been explored as a potential surrogate for salivary gland biopsies [8], the absence of a validated scoring system and inherent inter-observer variability restrict its use as a reliable tool. Non-invasive molecular imaging methods that can quantify function could be attractive tools for assessing disease status and potentially monitoring treatment effects.

This study assessed the potential of three functional imaging methods for the quantification of salivary gland structure, inflammation and function in patients with pSS. First, positron emission tomography-computed tomography (PET-CT) with  $^{11}\text{C}$ -methionine ( $^{11}\text{C}$ -MET) was used as a protein synthesis marker. As  $^{11}\text{C}$ -MET is prominently incorporated into cellular proteins [9, 10], it can assess residual salivary gland function. Second,  $^{18}\text{F}$ -fluorodeoxyglucose ( $^{18}\text{F}$ -FDG) PET-CT, which indicates metabolic tissue activity in tumours [11, 12] and inflammation due to the higher expression of glucose transporters and glycolytic index in inflammatory cells [4, 13–16], was used to assess glucose utilization. The ability to evaluate systemic manifestations of pSS using  $^{18}\text{F}$ -FDG was also examined [15]. Finally, multi-parametric MRI was conducted to assess gland inflammation, structure and function [17]. This is the first time  $^{11}\text{C}$ -MET has been used to characterize salivary gland inflammation and residual function in pSS.

## Methods

### Study design

The study (GSK study 203818; NCT02899377) duration was  $\leq 14$  weeks for patients with pSS, and  $\leq 11$  weeks for healthy volunteers (HVs). Study design (Supplementary Fig. S1, available at *Rheumatology* online) details are summarized in the Supplementary Methods, available at *Rheumatology* online.

### Endpoints

The primary endpoints were semi-quantitative parameters of  $^{11}\text{C}$ -MET and  $^{18}\text{F}$ -FDG uptake in submandibular and parotid salivary glands [standardized uptake value (SUV), tissue to reference ratio (T/R; an additional

measure that provides a semi-quantitative description of tracer kinetics), total inflammatory volume and quantitative parameters of inflammation and tissue microstructure derived from multi-parametric MRI in the salivary glands [exchange rate ( $K^{\text{trans}}$ ), apparent diffusion coefficient (ADC), pure diffusion coefficient (D) and microvascular volume fraction (f)] (see Image acquisition and analysis and Supplementary Materials, available at *Rheumatology* online).

Exploratory endpoints included  $^{11}\text{C}$ -MET and  $^{18}\text{F}$ -FDG uptake in lacrimal glands and association with markers of disease activity and lacrimal gland function, and further quantitative parameters of inflammation, function and structure derived from multi-parametric MRI of the salivary glands [Initial Rate of Enhancement, maximum enhancement, fat fraction (%), pseudo-diffusion ( $D^*$ ) and gland volume]. All secondary and exploratory endpoints are summarized in the Supplementary Materials, available at *Rheumatology* online.

### Ethical considerations

The study was performed in accordance with the principles of the International Council for Harmonization of Technical Requirements for Pharmaceuticals for Human Use, Good Clinical Practice, applicable country-specific requirements and the Declaration of Helsinki. The study was approved by the East of England – Cambridge East National Research Ethics Committee (REC No.: 16/EE/0296) and by the Administration of Radioactive Substances Advisory Committee (ARSAC), UK (Research Certificate No.: RPC 630/3925/35065). Written informed consent was obtained from all participants.

### Patient and public involvement

The informed consent form and study feasibility were reviewed by a group of patients before submission for ethical review.

### Study population

Eligible patients were  $\geq 30$  years, diagnosed with pSS according to the American-European Consensus Group criteria [18], with evidence of glandular reserve function (baseline unstimulated salivary flow of  $>0.0$  ml/min or stimulated baseline salivary flow  $>0.05$  mL/min). Patients also had systemically active disease defined by a EULAR Sjögren's Syndrome disease activity index (ESSDAI) score of  $\geq 5$  points.

Patients diagnosed with secondary SS or another systemic autoimmune disease, or who had a history of

malignancy  $\leq 5$  years before screening or unresolved acute or chronic infection were excluded.

HV were mean-age- and sex-matched to patients ( $\geq 40$  years for  $^{11}\text{C}$ -MET PET-CT plus MRI and  $\geq 30$  years for MRI without  $^{11}\text{C}$ -MET PET-CT).

Full inclusion and exclusion criteria are listed in the [Supplementary Materials](#), available at *Rheumatology* online.

### Image acquisition and analysis

At Visit 1, patients and HV underwent an MRI of the salivary glands and  $^{11}\text{C}$ -MET PET-CT (dynamic scan of the salivary glands followed by head-to-hip static scan); patients also underwent static  $^{18}\text{F}$ -FDG PET-CT (head-to-hip).  $^{11}\text{C}$ -MET PET-CT scans were acquired  $\sim 30$  min after a standardized light meal to stimulate salivary flow.  $^{18}\text{F}$ -FDG PET-CT scans were acquired after  $\geq 6$  h of fasting and 60 min after  $^{18}\text{F}$ -FDG administration. SUVs (SUVmax and SUVpeak) and volumes were automatically extracted for each region of interest following region of interest contouring. The parotid, submandibular and lacrimal glands were analysed using  $^{11}\text{C}$ -MET and  $^{18}\text{F}$ -FDG scans, as were the spleen, liver, thyroid and pancreas. Aorta blood pool was used as the reference region for T/R calculations. Total inflammatory volume was not calculated as there were no anatomically relevant areas indicative of inflamed tissue and/or focal uptake within the organs.

Multi-parametric MRI of the salivary glands included a T1w high resolution structural image, Dixon imaging, diffusion-weighted imaging, quantitative T1 mapping and dynamic contrast enhanced (DCE)-MRI, which took place following administration of a gadolinium-based contrast agent. Anatomical region of interests were defined on structural MRI for parotid and submandibular glands. Diffusion-weighted MRI imaging data were used to fit a multi-parametric intravoxel incoherent motion model [19], as well as a conventional diffusion model to estimate the apparent diffusion coefficient (ADC).

Full details of image acquisition and analysis are in the [Supplementary Materials](#), available at *Rheumatology* online.

### Clinical and histological evaluations

Clinical and biomarker assessments for patients and HV were performed at screening/baseline and Visit 2.

### Tear flow and salivary flow measurements

Lacrimal flow was measured using the Schirmer's test (unanaesthetized) and quantified as mean length wet per min (mm/min) over the two visits for each eye. Mean basal and stimulated (by paraffin chew) salivary flow were measured following standard procedures. Full details are given in the [Supplementary Materials](#), available at *Rheumatology* online.

### Salivary gland biopsy

Minor (labial) salivary gland biopsy was performed for patients at Visit 2. Salivary gland histological assessments included evaluation of focus score histological index (the number of mononuclear cell infiltrates containing  $\geq 50$  cells in a 4-mm<sup>2</sup> glandular tissue) [20] assessed on haematoxylin and eosin staining; and the detection of the immune infiltrate markers by immunofluorescence (CD20+ B cells, IgG+, IgA+, and IgM+ plasma cells [PC]). Slides from two cutting levels (100  $\mu\text{m}$  distance apart) were imaged using a NanoZoomer S60 digital slide scanner and NanoZoomer digital pathology viewer software version 2.6.13 (Hamamatsu Photonics K.K., Hamamatsu, Shizuoka, Japan). Immunofluorescence staining of CD3, CD20 and immunoglobulins was quantified using Fiji software [21] and the area fraction of each marker was expressed as the ratio of the stained area over the total area of salivary gland tissue. Full details are given in the [Supplementary Materials](#), including [Supplementary Table S1](#), available at *Rheumatology* online.

### Safety evaluations

Adverse events (AEs), pregnancies, vital signs and clinical laboratory tests were monitored throughout the study.

### Statistical analysis

Information on sample size is in the [Supplementary Materials](#), available at *Rheumatology* online. An exploratory comparison of patients vs HV was performed for each  $^{11}\text{C}$ -MET PET-CT and multi-parametric MRI derived quantitative parameter (data permitting), to estimate a difference (ratio where normality assumptions are not adequate) with 95% CI. Where 95% CI for difference were clearly above or below zero, this was described as higher/lower than the reference value. Pearson correlation (R) coefficient analyses were performed to assess the relationship between different imaging parameters and between imaging and clinical/histological parameters, as pre-specified in the reporting analysis plan. Correlations were defined as strong ( $R \geq 0.8$ ); moderate ( $R \geq 0.5$ ); or low ( $R \geq 0.2$ ). The study was not statistically powered to detect significant difference for any parameters.

## Results

### Participant disposition and baseline characteristics

Twenty-five participants were included; 12 patients and 13 HV ([Supplementary Fig. S2](#), available at *Rheumatology* online). Twelve HV completed MRI, of whom eight underwent  $^{11}\text{C}$ -MET PET-CT. One HV was withdrawn due to intolerance of the MRI (see Safety section). Patients and HV were well matched for age, sex and body weight; demographics are listed in [Table 1](#).

**TABLE 1** Demographics, baseline characteristics and disease characteristics of healthy volunteers and patients with pSS

| Demographics                                  | Healthy volunteers (n = 13) | Healthy volunteers who underwent <sup>11</sup> C-MET PET-CT scan (n = 8) | Patients with pSS (n = 12) | Overall (n = 25)   |
|---|-----------------------------|--|----------------------------|--------------------|
| Age, mean (s.d.), years <sup>a</sup>          | 48.1 (13.87)                | 51.5 (13.29)   | 49.0 (13.70)               | 48.5 (13.51)       |
| Sex, n (%)                                    |                             |  |                            |                    |
| Female  | 13 (100)                    | 8 (100)  | 12 (100)                   | 25 (100)           |
| BMI, mean (range), kg/m <sup>2</sup>          | 25.59 (20.7–34.1)           | 25.80 (20.7–34.1)  | 27.07 (20.0–39.4)          | 26.30 (20.0–39.4)  |
| Height, mean (range), cm                      | 167.5 (159–182)             | 168.4 (159–182)  | 162.8 (152–174)            | 165.2 (152–182)    |
| Weight, mean (range), kg                      | 72.33 (53.7–113.0)          | 73.99 (53.7–113.0)   | 71.53 (51.4–91.0)          | 71.95 (51.4–113.0) |
| Ethnicity, n (%)                              |                             |  |                            |                    |
| Not Hispanic or Latino                        | 13 (100)                    | 8 (100)  | 12 (100)                   | 25 (100)           |
| Race, n (%)                                   |                             |  |                            |                    |
| Black or African-American                     | 2 (15)                      | 1 (13)   | 0                          | 2 (8)              |
| Asian—Central/South Asian Heritage            | 0                           | 0  | 3 (25)                     | 3 (12)             |
| Asian—South-East Asian Heritage               | 0                           | 0  | 1 (8)                      | 1 (4)              |
| White—White/Caucasian/European Heritage       | 10 (77)                     | 7 (88)   | 5 (42)                     | 15 (60)            |
| Unknown                                       | 1 (8)                       | 0  | 3 (25)                     | 4 (16)             |
| Disease characteristics, mean (range)         |                             |  |                            |                    |
| Disease duration, years                       | —                           | —  | 5.8 (0.25–38.7)            | —                  |
| ESSDAI final score <sup>b</sup>               | —                           | —  | 8.6 (6–16)                 | —                  |
| ESSPRI final score <sup>c</sup>               | —                           | —  | 6.361 (4.33–8.33)          | —                  |
| Salivary flow rate <sup>d</sup> , ml/min      |                             |  |                            |                    |
| Basal unstimulated                            | 0.353 (0.20–0.62)           | —  | 0.193 (0.01–0.60)          | —                  |
| Stimulated                                    | 1.958 (0.91–3.41)           | —  | 0.728 (0.05–1.97)          | —                  |
| Difference <sup>e</sup>                       | 1.605 (0.63–3.21)           | —  | 0.535 (0.04–1.37)          | —                  |
| Strip length per minute <sup>f</sup> , mm/min |                             |  |                            |                    |
| Right eye                                     | 5.46 (0.80–23.60)           | —  | 1.72 (0–7.00)              | —                  |
| Left eye                                      | 4.89 (0.20–11.29)           | —  | 1.67 (0–7.00)              | —                  |
| Complement, g/l                               |                             |  |                            |                    |
| Component 3                                   | —                           | —  | 1.103 (0.77–1.62)          | —                  |
| Component 4 (n=11)                            | —                           | —  | 0.245 (0.07–0.39)          | —                  |
| IgG, g/l                                      | —                           | —  | 17.657 (6.70–26.73)        | —                  |

<sup>a</sup>Age imputed for missing date of birth.

<sup>b</sup>ESSDAI Final Score is the sum of 12 activity-level domain scores.

<sup>c</sup>ESSPRI Final Score is an average of pain, fatigue and dryness scales scores.

<sup>d</sup>Mean salivary flow rate calculated using screening and Visit 2 mean salivary flow.

<sup>e</sup>Difference is calculated by subtracting basal salivary flow rate from stimulated flow rate.

<sup>f</sup>Strip length wet per min (mm/min) calculated as length (mm) paper wet divided by time taken to wet (min).

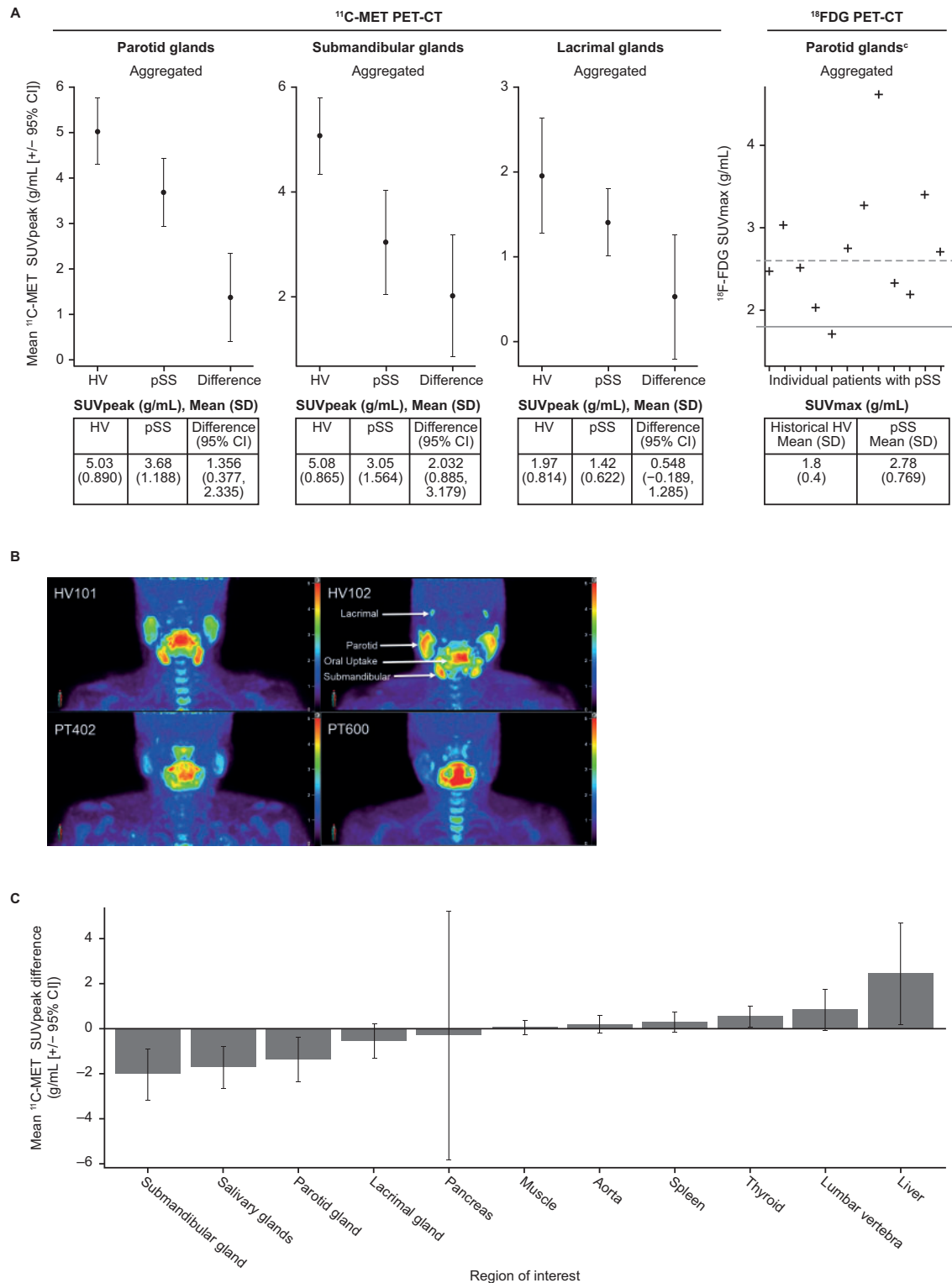
<sup>11</sup>C-MET: <sup>11</sup>C-Methionine; ESSDAI: EULAR Sjögren's Syndrome Disease Activity Index; ESSPRI: EULAR Sjögren's Syndrome Patient Reported Index; pSS: primary SS.

### Imaging methods reveal structural and metabolic differences between patients with pSS and HV

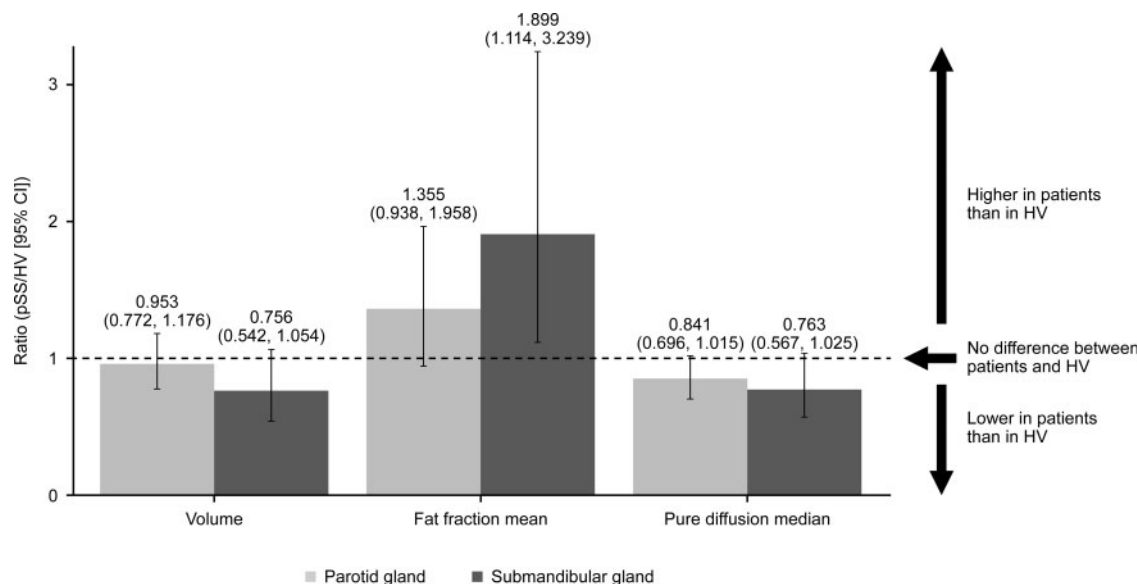
There was substantially lower <sup>11</sup>C-MET SUV<sub>peak</sub> uptake in the parotid and submandibular glands of patients compared with HV, while a similar trend towards lower uptake was observed for the lacrimal glands, indicating reduced protein synthesis (Fig. 1, Supplementary Fig. S3A and B and Supplementary Video S1, available at *Rheumatology* online). T/R data were consistent with <sup>11</sup>C-MET SUV<sub>peak</sub> findings (Supplementary Table S2, available at *Rheumatology* online). Higher <sup>11</sup>C-MET SUV<sub>peak</sub> uptake was seen in the thyroid and liver of

patients vs HV, with trends towards higher uptake also seen in the spleen and lumbar vertebrae (Fig. 1C), suggesting increased metabolic activity in these organs, although this requires further confirmation.

<sup>18</sup>F-FDG SUV<sub>max</sub> was numerically higher in the parotid glands of patients compared with historical HV, indicating higher glycolytic activity in the salivary glands of patients (Fig. 1A) [15, 22]. Historical data for submandibular <sup>18</sup>F-FDG uptake were not available. <sup>18</sup>F-FDG SUV<sub>peak</sub> values for parotid and submandibular glands are shown in Supplementary Fig. S3C and D, available at *Rheumatology* online. Uptake of <sup>18</sup>F-FDG outside of salivary glands in patients with pSS was reviewed;

**Fig. 1**  $^{11}\text{C}$ -MET and  $^{18}\text{F}$ -FDG uptake between patients with pSS and HVs

**(A)**  $^{11}\text{C}$ -MET SUVpeak in parotid, submandibular and lacrimal glands (pSS and HV) and  $^{18}\text{F}$ -FDG SUVmax in parotid glands (pSS)<sup>a</sup>; **(B)** dynamic imaging (summations of the final 10 minutes, approx. 30–40 minutes post injection) of  $^{11}\text{C}$ -MET uptake in parotid, submandibular and lacrimal glands for HVs (top) and patients with pSS (bottom). **(C)** Point estimate (95% CI) of mean SUVpeak difference (pSS-HV) for  $^{11}\text{C}$ -MET<sup>b</sup>. <sup>a</sup>Aggregated includes left and right salivary gland parameters. Difference is difference between means. <sup>b</sup>For  $^{11}\text{C}$ -MET SUVmax data, see [Supplementary Fig. S7](#), available at *Rheumatology* online. <sup>c</sup>Grey horizontal line indicates historical max SUV (mean [solid line]; +2SD [dotted line]) Basu S, Houseni M, Alavi A. Significance of incidental fluorodeoxyglucose uptake in the parotid glands and its impact on patient management. *Nucl Med Commun* 2008;29:367–73.  $^{11}\text{C}$ -MET:  $^{11}\text{C}$ -Methionine;  $^{18}\text{F}$ -FDG:  $^{18}\text{F}$ -fluorodeoxyglucose; HV: healthy volunteer; Max: maximum; pSS: primary SS; SUV: standardized uptake value.

**Fig. 2** Differences in multi-parametric MRI measures between patients with pSS and HV

Point estimate (95% CI) of the geometric mean ratio (pSS/HV)<sup>a</sup> gland volume (cm<sup>3</sup>), fat fraction mean (%) and pure diffusion median (10<sup>-3</sup>mm<sup>2</sup>/s) in the parotid and submandibular glands from the multi-parametric MRI scan. Ratios are derived from the back-transformed estimate of the difference (pSS – HV) between log transformed means, and 95% CI are derived from the back-transformed estimate of the log 95% CI. CI is calculated using the Satterthwaite approximation. HV: healthy volunteer; pSS: primary SS.

however, no clinically important findings were reported following radiologist review. <sup>18</sup>F-FDG uptake in different regions of interest is shown in [Supplementary Table S3](#), available at *Rheumatology* online.

A substantially lower submandibular gland, but not parotid gland, volume compared with HVs ([Fig. 2](#)) was observed on MR volumetric assessment. Furthermore, median (IQR) MRI fat fraction was higher in both the parotid and submandibular glands of patients [36.4 (26.6, 52.1) and 21.8 (12.7, 35.1), respectively] relative to HV [28.8 (20.4, 32.4) and 10.6 (9.9, 12.5), respectively], possibly reflecting some fat replacement of functional gland tissue in patients with pSS ([Fig. 2](#)). Patients also demonstrated greater variability around the point estimate of the fat fraction, compared with HV. Substantially lower pure diffusion was also observed in the parotid [mean (s.d.): 0.676 (0.1515)] and submandibular glands [0.807 (0.3001)] of patients compared with HV [0.787 (0.0950) and 0.993 (0.1415), respectively] ([Fig. 2](#)), possibly reflecting higher cell density. Additional MRI parameters are presented in [Supplementary Fig. S4](#), available at *Rheumatology* online.

Findings in the parotid glands of patients and HV from either PET-CT or MRI were symmetrical when comparing left/right ([Supplementary Fig. S5](#), available at *Rheumatology* online).

In HV, <sup>11</sup>C-MET SUVpeak uptake was similar between parotid and submandibular glands. However, in patients, <sup>11</sup>C-MET SUVpeak uptake was lower in submandibular compared with parotid glands, suggesting that protein synthesis in the submandibular glands was

disproportionately affected in this group of pSS patients. However, <sup>18</sup>F-FDG SUVpeak uptake was similar in the submandibular and parotid glands of patients.

#### Correlations between imaging methods

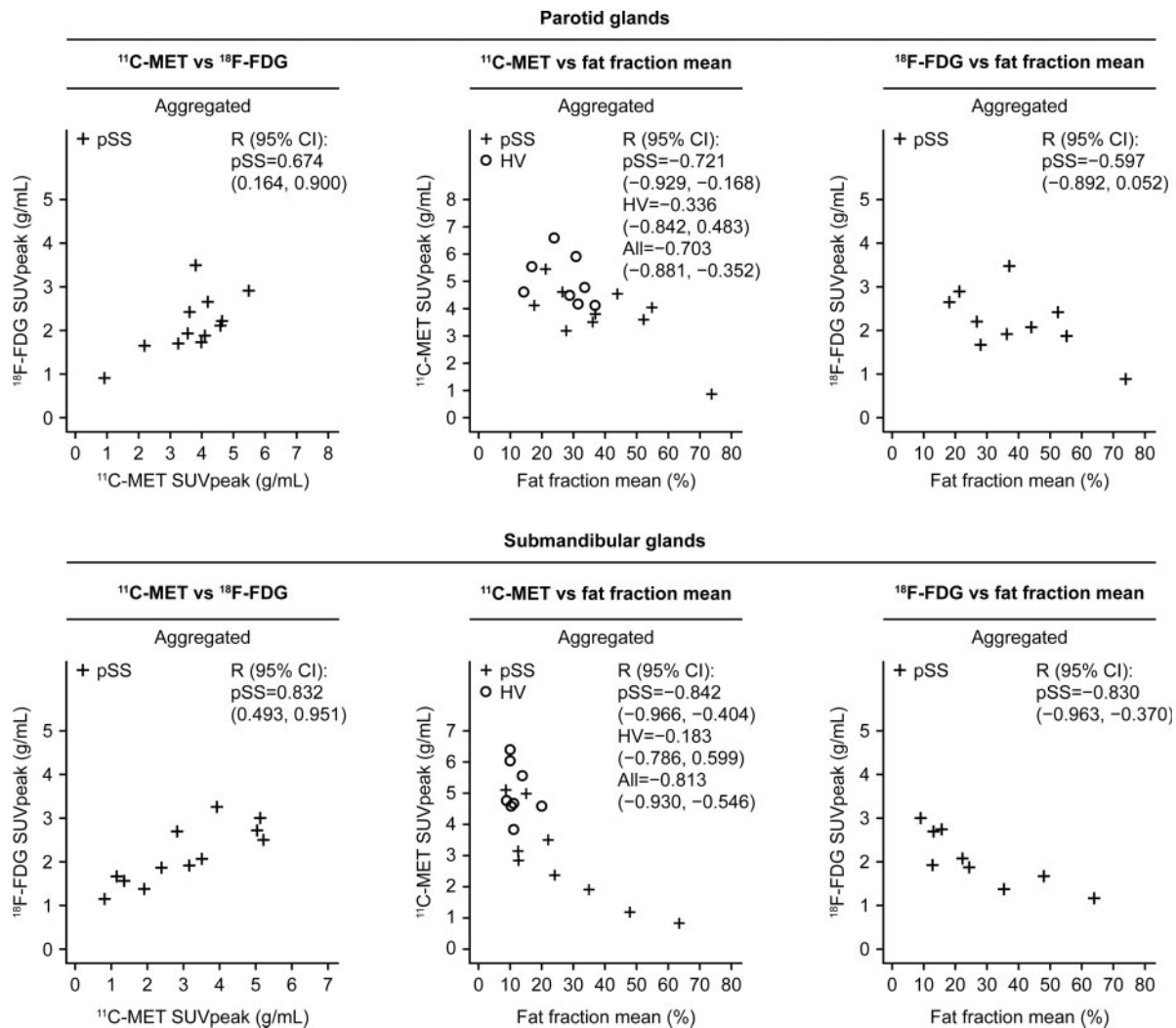
<sup>11</sup>C-MET and <sup>18</sup>F-FDG SUVpeak uptake were positively correlated in the parotid and submandibular glands of patients ([Fig. 3](#)). <sup>11</sup>C-MET and <sup>18</sup>F-FDG SUVpeak displayed inverse strong and moderate correlations, respectively, with fat fraction in both submandibular and parotid glands of patients; again, this correlation was strongest in the submandibular glands ([Fig. 3](#)). <sup>11</sup>C-MET displayed weakly negative correlations with fat fraction in the parotid and submandibular glands of HV ([Fig. 3](#)).

#### Correlations between imaging data and disease characteristics and histological measures

##### Imaging vs disease characteristics

In keeping with loss of salivary gland function over time in patients with pSS, <sup>11</sup>C-MET uptake was strongly negatively correlated with disease duration. Similarly, there was moderate negative correlation of <sup>18</sup>F-FDG uptake with time ([Fig. 4A](#)). In agreement with the PET findings, MRI fat fraction was moderately positively correlated with disease duration ([Fig. 4A](#)), while a strong negative correlation was observed for MRI pure diffusion median vs disease duration [−0.808 (−0.948, −0.403)].

Salivary flow was uniformly low in patients, and <sup>11</sup>C-MET and <sup>18</sup>F-FDG SUVpeak demonstrated only a weak positive correlation, or no correlation, with mean

**Fig. 3** Correlations between  $^{11}\text{C}$ -MET,  $^{18}\text{F}$ -FDG and MRI fat fraction imaging parameters

$^{11}\text{C}$ -MET:  $^{11}\text{C}$ -methionine;  $^{18}\text{F}$ -FDG:  $^{18}\text{F}$ -fluorodeoxyglucose; HV: healthy volunteer; pSS, primary SS; R, Pearson's correlation; SUV: standardized uptake value

stimulated salivary flow rate in the parotid glands of patients (Fig. 4B). In contrast, lacrimal gland  $^{11}\text{C}$ -MET SUVpeak positively correlated (strongly and moderately) with tear flow rates in patients; however, none or weak correlations were observed for HV (Fig. 4C).

Further correlation data can be found in Supplementary Table S4, available at *Rheumatology* online.

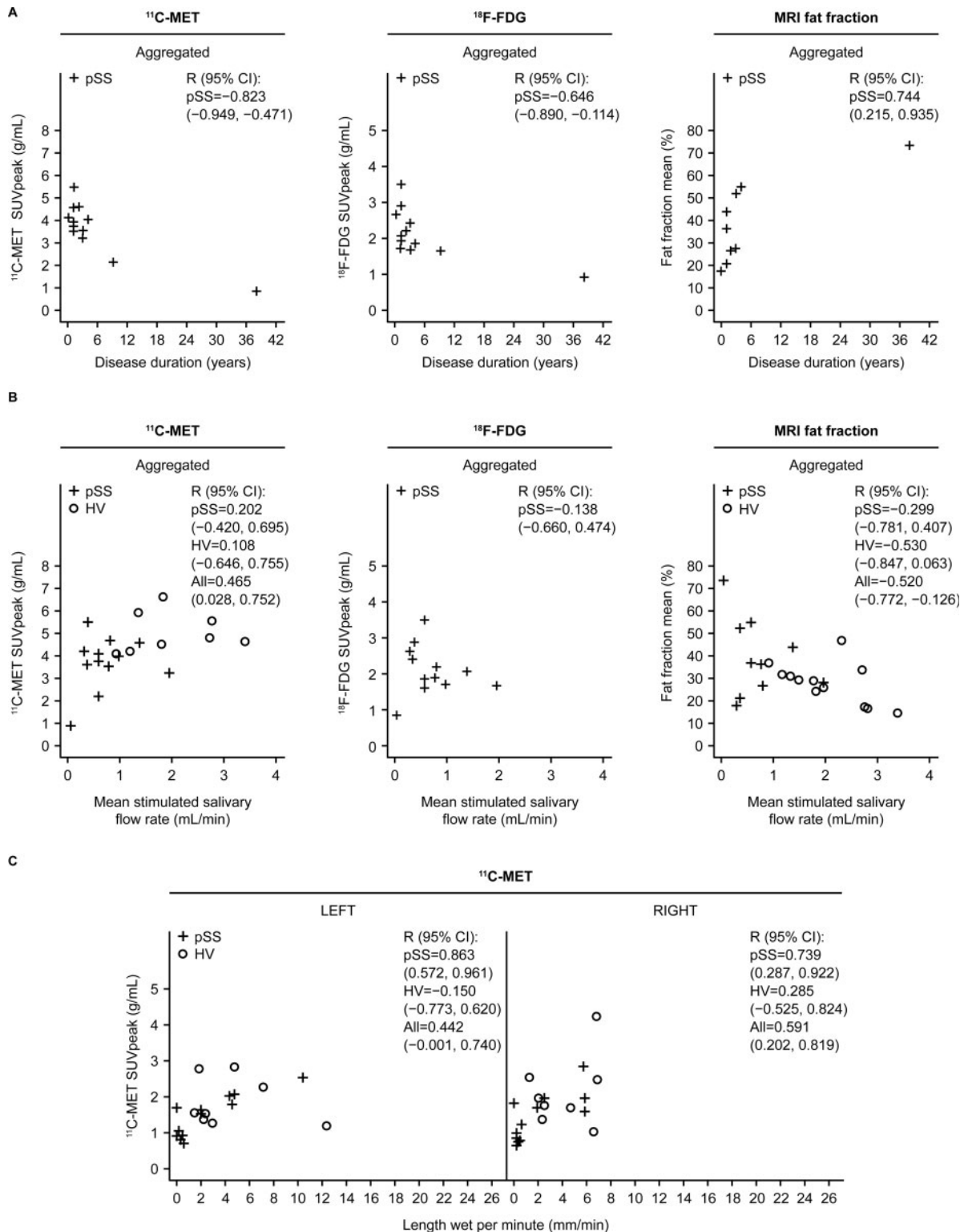
#### Imaging vs histological measures

Surprisingly, histological focus scores from minor salivary gland biopsy demonstrated no clear correlation with either  $^{11}\text{C}$ -MET or  $^{18}\text{F}$ -FDG SUVpeak in patients (Fig. 5A). A moderate positive correlation was observed between  $^{18}\text{F}$ -FDG SUVpeak in the parotid gland and CD20+ B-cell infiltration (or area fraction) in the minor salivary gland of patients, suggesting that increased FDG activity is reflective of a B-cell tissue

infiltrate. However, there was no such correlation between  $^{11}\text{C}$ -MET SUVpeak and CD20 (Fig. 5B), suggesting that methionine activity is not confounded by inflammation.

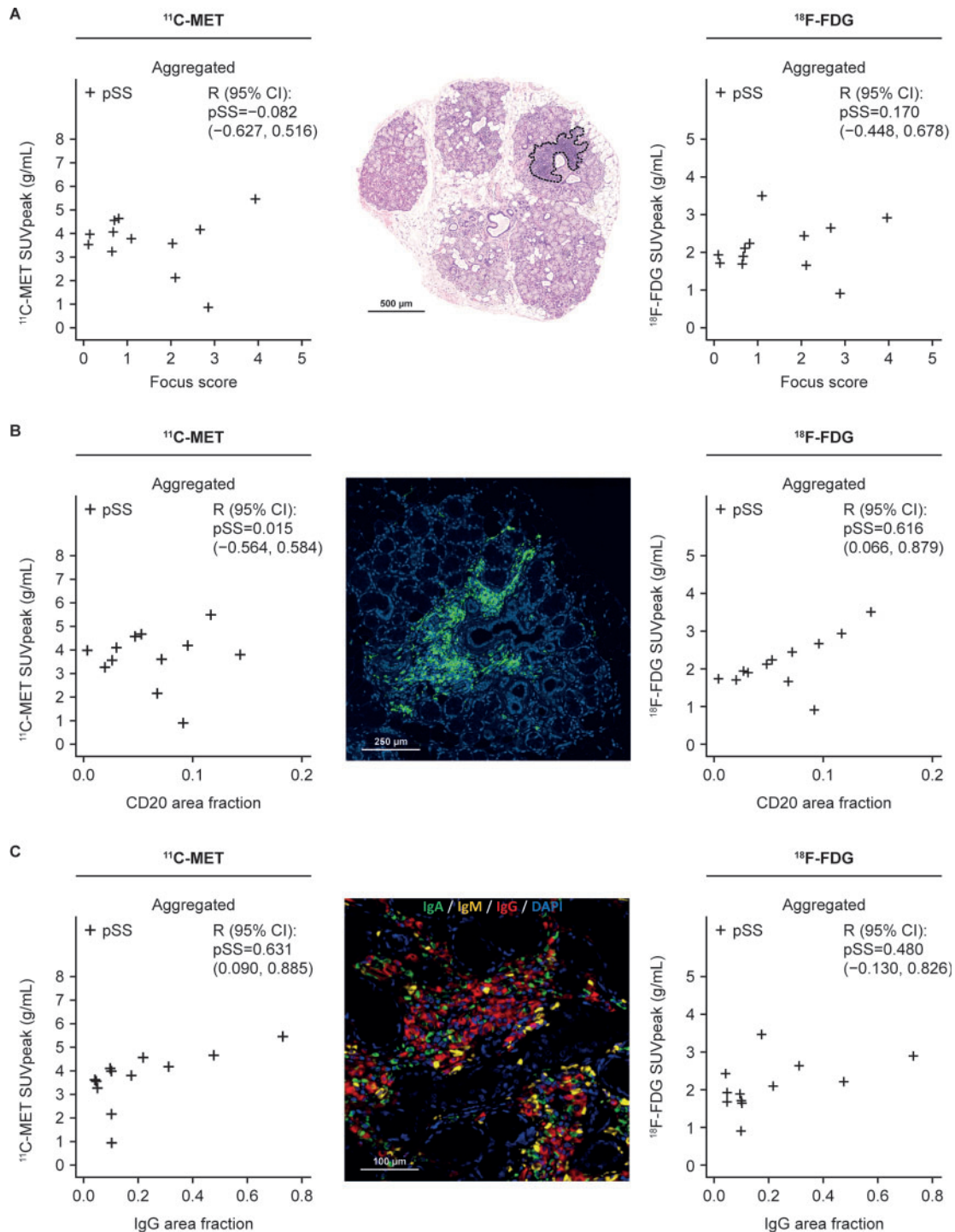
In the parotid gland of patients, moderate positive correlations were noted between IgG deposition in minor salivary gland biopsies, and both  $^{11}\text{C}$ -MET and  $^{18}\text{F}$ -FDG SUVpeak (Fig. 5C). Additionally, a moderate positive correlation was shown between minor salivary gland IgM and parotid gland  $^{11}\text{C}$ -MET SUVpeak [R (95% CI): 0.505 (-0.097, 0.836)] and a moderate negative correlation was shown between minor salivary gland IgM and fat fraction [R (95% CI): -0.503 (-0.860, 0.185)] in the parotid gland. Minor salivary gland IgA was also moderately positively correlated with  $^{11}\text{C}$ -MET SUVpeak [R (95% CI): 0.628 (0.085, 0.884)] in the parotid gland.

**Fig. 4** Correlations between  $^{11}\text{C}$ -MET and  $^{18}\text{F}$ -FDG uptake and MRI fat fraction with disease characteristics



$^{11}\text{C}$ -MET and  $^{18}\text{F}$ -FDG peak SUV and MRI fat fraction correlations with (A) disease duration (years) and (B) stimulated salivary flow rate and (C) correlation of tear flow with  $^{11}\text{C}$ -MET PET-CT peak SUV in the lacrimal gland. Data were available for 10 patients only.  $^{11}\text{C}$ -MET:  $^{11}\text{C}$ -methionine;  $^{18}\text{F}$ -FDG:  $^{18}\text{F}$ -fluorodeoxyglucose; HV: healthy volunteer; pSS: primary SS; R, Pearson's correlation; SUV: standardized uptake value.



**Fig. 5** Correlations between  $^{11}\text{C}$ -MET and  $^{18}\text{F}$ -FDG uptake with histological markers

**(A)**  $^{11}\text{C}$ -MET and  $^{18}\text{F}$ -FDG SUVpeak in parotid gland correlations with focus score; representative histological image of minor salivary gland lobule stained for haematoxylin and eosin (H&E) for focus score assessment. Highlighted section identifies an inflammatory focus, defined as an aggregate of at least 50 inflammatory mononuclear cells. **(B)**  $^{11}\text{C}$ -MET and  $^{18}\text{F}$ -FDG SUVpeak in parotid gland correlated with CD20; representative immunofluorescence staining for CD20 identifying B cells within inflammatory aggregates in pSS. **(C)**  $^{11}\text{C}$ -MET and  $^{18}\text{F}$ -FDG SUVpeak in parotid gland correlated with IgG in minor salivary gland; representative immunofluorescence staining for IgA, IgG and IgM, expressed by plasma cells in pSS.  $^{11}\text{C}$ -MET:  $^{11}\text{C}$ -methionine;  $^{18}\text{F}$ -FDG:  $^{18}\text{F}$ -fluorodeoxyglucose; HV: healthy volunteer; pSS, primary SS; R, Pearson's correlation; SUV: standardized uptake value.

## Safety

Overall, study procedures were well tolerated. Four patients and two HV reported AEs most commonly headache, reported in one patient and one HV (Supplementary Table S5, available at *Rheumatology* online). Most AEs were mild in intensity. One HV was withdrawn from the study because of hyperaesthesia and paraesthesia experienced during the MRI scan; these AEs were moderate in intensity and deemed unrelated to the study procedures. No deaths or serious AEs were reported.

## Discussion

This is the first evaluation of the amino acid PET tracer  $^{11}\text{C}$ -MET in patients with pSS. Additionally, the application of MRI and  $^{18}\text{F}$ -FDG PET-CT to quantify and characterize disease manifestations in pSS were evaluated in this imaging/histology comparative study.

Lower  $^{11}\text{C}$ -MET uptake was observed in the submandibular and parotid glands of patients compared with HV, in addition to a trend towards lower uptake in the lacrimal glands, suggesting lower protein synthesis in patients than in HV. Although  $^{11}\text{C}$ -MET data alone do not distinguish whether such protein synthesis would be attributable to synthesis of saliva or inflammation, the lower uptake would be consistent with loss of glandular function [9, 10]. Together with the strong negative correlation between disease duration and  $^{11}\text{C}$ -MET uptake in the parotid gland, and the correlations between  $^{11}\text{C}$ -MET uptake and lacrimal tear flow, our findings suggest that reduced  $^{11}\text{C}$ -MET uptake is a marker of residual gland function. Notable confounding factors may be the tendency for older participants to have longer disease duration and the known minor decline in salivary gland function with age, even in healthy individuals [23], although patients were age-matched to HV.

Surprisingly,  $^{11}\text{C}$ -MET uptake did not correlate with salivary flow rates, possibly due to the impact of factors other than gland function on salivary flow (e.g. diurnal variation in flow rates, patients' hydration status at time of collection, pH and viscosity of saliva, dental plaque status, tongue pressure and coating status). One possibility is that gland inflammation itself can reduce salivary gland function, independent of loss of protein synthetic activity. However, salivary flow rate data for patients with pSS were skewed towards low values, thus affecting quantitation accuracy as the correlation estimations assume normal distribution; therefore, these results should be interpreted with caution.

Parotid gland  $^{18}\text{F}$ -FDG uptake tended to be higher in patients with pSS compared with previously published control data [22, 24]; and there was a moderate negative correlation with disease duration, whilst a positive correlation was observed with  $^{11}\text{C}$ -MET uptake. It is worth noting that patients with pSS were at different disease stages and overall displayed high  $^{18}\text{F}$ -FDG uptake and

lower  $^{11}\text{C}$ -MET uptake compared with HV, consistent with greater salivary gland inflammation and loss of functional reserve. The positive correlation between  $^{18}\text{F}$ -FDG and  $^{11}\text{C}$ -MET in patients with pSS can be explained by considering overall disease course, in which it is expected that both  $^{18}\text{F}$ -FDG and  $^{11}\text{C}$ -MET uptake declines from high to normal ( $^{18}\text{F}$ -FDG) and normal to low ( $^{11}\text{C}$ -MET) as the disease progresses, respectively (Supplementary Fig. S6, available at *Rheumatology* online), as is supported by the study data (Fig. 4A). Overall, we hypothesize that inflammation occurs early in the disease course and is associated with relatively preserved underlying gland function, which transitions to a decline in both inflammation and gland function from early to late disease, thereby explaining the positive correlation between the  $^{18}\text{F}$ -FDG and  $^{11}\text{C}$ -MET imaging parameters. Alternatively, both tracers could be primarily affected by cellular integrity, rather than  $^{18}\text{F}$ -FDG being a measure of inflammation, and  $^{11}\text{C}$ -MET of function. Notably, leucocyte infiltration has not been reported to increase  $^{11}\text{C}$ -MET uptake to the same degree as  $^{18}\text{F}$ -FDG [25]. However, there were stronger correlations of  $^{18}\text{F}$ -FDG with markers of inflammation (CD20+ B-cell infiltration) and  $^{11}\text{C}$ -MET with accepted markers of function (tear flow), suggesting that they measure different aspects of disease. Parotid gland  $^{18}\text{F}$ -FDG uptake did not correlate with histological focus score on minor salivary gland biopsy. It is unclear why such a correlation could not be observed, as it has been demonstrated that minor salivary gland focus score correlates with inflammation in parotid glands in an ultrasound study [26]. Furthermore, moderate correlations were seen with CD20 infiltration and IgG deposition in minor salivary gland, supporting the hypothesis that  $^{18}\text{F}$ -FDG uptake may be a measure of inflammation; however, this may be due to sample size.

Outside of the salivary glands,  $^{11}\text{C}$ -MET uptake was higher in the thyroid and liver of patients with pSS compared with HV, suggesting increased protein synthesis. Although no patients with pSS were reported to be clinically affected by thyroiditis, an association between thyroid disease, most frequently subclinical hypothyroidism, and pSS has been reported [27]; however, this was not supported by the physiological levels of  $^{18}\text{F}$ -FDG uptake in the thyroids of corresponding patients in our study. Overall, the small sample size prevents further conclusions being drawn.

Variable  $^{18}\text{F}$ -FDG uptake was observed across multiple organs, but no findings were considered clinically abnormal. In contrast, a study by Cohen *et al.* [15] observed abnormal uptake in organs including lung, lymph nodes and thyroid. However, the patient subsets recruited included those with lung involvement and suspected lymphoma, whereas clinical suspicion of lymphoma was an exclusion criterion for this study. Furthermore, methods of analysis and definitions of positive uptake differed between the studies.

The Dixon method, used to estimate fat fraction from structural MRI, has previously been used to successfully

measure the characteristic fat deposition in the parotid glands of patients with pSS [28]. Diffusion-weighted imaging and entropy of parotid glands previously enabled discrimination between patients with active and non-active pSS [29]. In this study, evidence from MRI, including higher fat fraction and lower pure diffusion in the glands of patients compared with HV and correlation of both fat fraction and pure diffusion (positive and negative, respectively) with disease duration, is suggestive of fatty replacement of functional gland tissue, which has been shown to occur as glandular atrophy and disease progression occurs. Fat fraction was also negatively correlated with  $^{11}\text{C}$ -MET and  $^{18}\text{F}$ -FDG uptake. Together, these data support the use of MRI, particularly fat fraction and pure diffusion parameters, in the non-invasive characterization of pSS. These findings are consistent with a small study that demonstrated a correlation between MRI findings and disease stage in patients with secondary SS [30].

Overall, these results corroborate a hypothesis in which pSS may start with inflammatory reactions that are followed by deterioration of salivary and lacrimal gland function and a gradual atrophy that includes replacement of glandular cells with fat [31]. The observation of retained right-left symmetry, which is consistent with previous work [10], indicates that the disease is global and not sporadically attacking one specific gland. Intra-individual differences seen in imaging parameters of parotid and submandibular glands indicate that the disease manifestation may separately affect the parotid or submandibular glands to different degrees.

Study limitations include the use of historical control data for the  $^{18}\text{F}$ -FDG analyses, which did not allow precise comparisons between patients and controls, and analysis of correlations between imaging vs function/clinical parameters in the parotid gland only (for technical reasons for DCE-MRI and to limit the number of comparisons conducted). However, with a few exceptions, the major findings between the parotid and submandibular glands were similar. Parotid imaging parameters only were correlated with overall salivary flow, although the disease generally does involve both parotid and submandibular glands. Finally, the imaging techniques used were not compared with ultrasound examination of the salivary glands.

In conclusion,  $^{11}\text{C}$ -MET scans of the salivary and lacrimal glands in patients with pSS have the potential to quantitatively assess residual function in individual glands, while  $^{18}\text{F}$ -FDG is a potential method to assess salivary gland inflammation. These imaging modalities may facilitate non-invasive assessment of patients with pSS, particularly in early phase clinical trials.  $^{11}\text{C}$ -MET PET-CT,  $^{18}\text{F}$ -FDG PET-CT and MRI fat fraction could be used to define patients with inflammation (as measured by increased  $^{18}\text{F}$ -FDG uptake) along with relatively preserved residual salivary gland function (preserved  $^{11}\text{C}$ -MET uptake) as opposed to patients with severe dysfunction; the former 'sub-group' potentially being better candidates for drug therapy. Additionally,

although not evaluated here, some of these parameters could be used in future interventional studies to assess the mechanistic effects of therapeutic interventions, complementing clinical scoring.

## Acknowledgements

M.Bo., C.C., A.S., T.F., K.P., N.R. and R.T. contributed to conception or design, acquisition of data and data analysis or interpretation; M.K., A.R.T. and E.P. contributed to acquisition of data and data analysis or interpretation; N.J., A.vM., R.J., P.G., G.S., N.P., L.K., C.G., M.dG., N.W., M.Be. and P.J.-R. contributed to conception or design and data analysis or interpretation. D.L. contributed to data analysis or interpretation. GSK is committed to publicly disclosing the results of GSK-sponsored clinical research and research that evaluates GSK medicines, and as such was involved in the decision to submit. Study documents can be requested for further research from [www.clinicalstudydatarequest.com](http://www.clinicalstudydatarequest.com). Researchers can enquire about the availability of data from GSK clinical studies that are not listed on the site before they submit a research proposal. The authors would like to acknowledge the contribution of Elisa Astorri; Rohini Akosa, clinical study co-ordinator; Ryan Janisch, PET technologist; Mark Tanner, MR radiographer; and other clinical and imaging staff who assisted with this study at Invicro. Medical writing support was provided by Sam Halliwell, PhD, of Fishawack Indicia Ltd, UK.

**Funding:** This study was funded by GlaxoSmithKline (GSK).

**Disclosure statement:** T.F., K.P., N.R., A.vM., R.J., P.G., M.dG., N.P., N.W., P.J.-R. and R.T. are employees of GSK and hold stocks and shares in the company; M.Be. acted as external consultant to GSK; M.K. is an NHS consultant seconded to the GSK Clinical Unit Cambridge (50%) and has nothing to disclose; A.S. and G.S. are ex-employees of GSK; the other authors have declared no conflicts of interest.

## Data availability statement

GSK is committed to publicly disclosing the results of GSK-sponsored clinical research and research that evaluates GSK medicines, and as such was involved in the decision to submit. Study documents can be requested for further research from [www.clinicalstudydatarequest.com](http://www.clinicalstudydatarequest.com). Researchers can enquire about the availability of data from GSK clinical studies that are not listed on the site before they submit a research proposal.

## Supplementary data

Supplementary data are available at *Rheumatology* online.

## References

- 1 Fox RI. Sjogren's syndrome. *Lancet* 2005;366:321–31.
- 2 de Sousa Gomes P, Juodzbaly G, Fernandes MH, Guobis Z. Advances in the aetiopathogenesis of Sjogren's syndrome: a literature review. *J Oral Maxillofac Res* 2012;3:e2.
- 3 Nocturne G, Mariette X. Sjogren Syndrome-associated lymphomas: an update on pathogenesis and management. *Br J Haematol* 2015;168:317–27.
- 4 Ziakas PD, Poulou LS, Thanos L. Towards integrating positron emission tomography for work-up of patients with Sjogren's syndrome and associated lymphomas. *Autoimmun Rev* 2014;13:327–9.
- 5 Stefanski AL, Tomiak C, Pleyer U *et al.* The diagnosis and treatment of Sjogren's syndrome. *Dtsch Arztebl Int* 2017;114:354–61.
- 6 Seror R, Bowman SJ, Brito-Zeron P *et al.* EULAR Sjögren's syndrome disease activity index (ESSDAI): a user guide. *RMD Open* 2015;1:e000022.
- 7 Shiboski CH, Shiboski SC, Seror R *et al.* 2016 ACR-EULAR classification criteria for primary Sjögren's syndrome: a consensus and data-driven methodology involving three international patient cohorts. *Arthritis Rheumatol* 2017;69:35–45.
- 8 Jonsson MV, Baldini C. Major salivary gland ultrasonography in the diagnosis of Sjogren's syndrome: a place in the diagnostic criteria? *Rheum Dis Clin North Am* 2016;42:501–17.
- 9 Glaudemans AW, Enting RH, Heesters MA *et al.* Value of 11C-methionine PET in imaging brain tumours and metastases. *Eur J Nucl Med Mol Imaging* 2013;40: 615–35.
- 10 Harris SM, Davis JC, Snyder SE *et al.* Evaluation of the biodistribution of 11C-methionine in children and young adults. *J Nucl Med* 2013;54:1902–8.
- 11 Kubota R, Yamada S, Kubota K *et al.* Intratumoral distribution of fluorine-18-fluorodeoxyglucose in vivo: high accumulation in macrophages and granulation tissues studied by microautoradiography. *J Nucl Med* 1992;33:1972–80.
- 12 Vander Heiden MG, Cantley LC, Thompson CB. Understanding the Warburg effect: the metabolic requirements of cell proliferation. *Science* 2009;324: 1029–33.
- 13 Keraen J, Blanc E, Besson FL *et al.* Usefulness of (18) F-labeled fluorodeoxyglucose-positron emission tomography for the diagnosis of lymphoma in primary Sjogren's syndrome. *Arthritis Rheumatol* 2019;71: 1147–57.
- 14 Poulou LS, Ziakas PD, Papageorgiou M *et al.* FDG-PET/CT in the post-therapy evaluation of salivary gland lymphomas in Sjogren's syndrome: a prospective study. *Eur Congress Radiol* 2013; Poster Number C-0355.
- 15 Cohen C, Mekinian A, Uzunhan Y *et al.* 18F-fluorodeoxyglucose positron emission tomography/computer tomography as an objective tool for assessing disease activity in Sjogren's syndrome. *Autoimmun Rev* 2013;12:1109–14.
- 16 Yamada S, Kubota K, Kubota R, Ido T, Tamahashi N. High accumulation of fluorine-18-fluorodeoxyglucose in turpentine-induced inflammatory tissue. *J Nucl Med* 1995;36:1301–6.
- 17 Buus S, Grau C, Munk OL *et al.* 11C-methionine PET, a novel method for measuring regional salivary gland function after radiotherapy of head and neck cancer. *Radiother Oncol* 2004;73:289–96.
- 18 Vitali C, Bombardieri S, Jonsson R *et al.* Classification criteria for Sjogren's syndrome: a revised version of the European criteria proposed by the American-European Consensus Group. *Ann Rheum Dis* 2002;61:554–8.
- 19 Le Bihan D, Breton E, Lallemand D *et al.* Separation of diffusion and perfusion in intravoxel incoherent motion MR imaging. *Radiology* 1988;168:497–505.
- 20 Fisher BA, Jonsson R, Daniels T *et al.* Standardisation of labial salivary gland histopathology in clinical trials in primary Sjögren's syndrome. *Ann Rheum Dis* 2017;76: 1161–8.
- 21 Schindelin J, Arganda-Carreras I, Frise E *et al.* Fiji: an open-source platform for biological-image analysis. *Nat Methods* 2012;9:676–82.
- 22 Basu S, Houseni M, Alavi A. Significance of incidental fluorodeoxyglucose uptake in the parotid glands and its impact on patient management. *Nucl Med Commun* 2008;29:367–73.
- 23 Su GY, Wang CB, Hu H *et al.* Effect of laterality, gender, age and body mass index on the fat fraction of salivary glands in healthy volunteers: assessed using iterative decomposition of water and fat with echo asymmetry and least-squares estimation method. *Dentomaxillofac Radiol* 2019;48:20180263.
- 24 Nakamoto Y, , Tatsumi M, , Hammoud D, *et al.* Normal FDG distribution patterns in the head and neck: PET/CT Evaluation. *Radiology* 2005;234:879–85.
- 25 Oka S, Okudaira H, Ono M *et al.* Differences in transport mechanisms of trans-1-amino-3-[18 F] fluorocyclobutanecarboxylic acid in inflammation, prostate cancer, and glioma cells: comparison with L-[Methyl-11 C] methionine and 2-deoxy-2-[18 F] fluoro-D-glucose. *Mol Imaging Biol* 2014;16:322–9.
- 26 Ali S, Brown J, Ngu R, Daniels T, Greenspan J, Odell E. Correlation between ultrasound imaging of major salivary glands and histopathological findings of labial gland biopsy samples in Sjogren's syndrome. *Lancet* 2013; S19. <https://www.thelancet.com/pdfs/journals/lancet/PIIS0140673613604596.pdf>.
- 27 Jara LJ, Navarro C, Brito-Zeron M del P *et al.* Thyroid disease in Sjogren's syndrome. *Clin Rheumatol* 2007;26: 1601–6.
- 28 Chikui T, Yamashita Y, Kise Y *et al.* Estimation of proton density fat fraction of the salivary gland. *Br J Radiol* 2018;91:20170671.
- 29 Chu C, Wang F, Zhang H *et al.* Whole-volume ADC histogram and texture analyses of parotid glands as an

- image biomarker in evaluating disease activity of primary Sjogren's syndrome. *Sci Rep* 2018;8:15387.
- 30 Yokosawa M, Tsuboi H, Nasu K *et al.* Usefulness of MR imaging of the parotid glands in patients with secondary Sjogren's syndrome associated with rheumatoid arthritis. *Mod Rheumatol* 2015;25:415–20.
- 31 Skarstein K, Aqrabi LA, Oijordsbakken G, Jonsson R, Jensen JL. Adipose tissue is prominent in salivary glands of Sjogren's syndrome patients and appears to influence the microenvironment in these organs. *Autoimmunity* 2016;49:338–46.